Association of the receptor for activated C-kinase 1 with ribosomes in *Plasmodium falciparum*

Jessey Erath[ORCID] **and Sergej Djuranovic**[*][ORCID]

From the Department of Cell Biology and Physiology, Washington University School of Medicine, St Louis, Missouri, USA

Edited by Ronald Wek

The receptor for activated C-kinase 1 (RACK1), a highly conserved eukaryotic protein, is known to have many varying biological roles and functions. Previous work has established RACK1 as a ribosomal protein, with defined regions important for ribosome binding in eukaryotic cells. In *Plasmodium falciparum*, RACK1 has been shown to be required for parasite growth, however, conflicting evidence has been presented about RACK1 ribosome binding and its role in mRNA translation. Given the importance of RACK1 as a regulatory component of mRNA translation and ribosome quality control, the case could be made in parasites that RACK1 either binds or does not bind the ribosome. Here, we used bioinformatics and transcription analyses to further characterize the *P. falciparum* RACK1 protein. Based on homology modeling and structural analyses, we generated a model of *P. falciparum* RACK1. We then explored mutant and chimeric human and *P. falciparum* RACK1 protein binding properties to the human and *P. falciparum* ribosome. We found that WT, chimeric, and mutant RACK1 exhibit distinct ribosome interactions suggesting different binding characteristics for *P. falciparum* and human RACK1 proteins. The ribosomal binding of RACK1 variants in human and parasite cells shown here demonstrates that although RACK1 proteins have highly conserved sequences and structures across species, ribosomal binding is affected by species-specific alterations to this protein. In conclusion, we show that in the case of *P. falciparum*, contrary to the structural data, RACK1 is found to bind ribosomes and actively translating polysomes in parasite cells.

RACK1 is a highly conserved, eukaryotic, seven-bladed WD β-propeller repeat scaffolding protein (1). The WD domain proteins, fold into a β-propeller structure, is typically characterized by the repetition of glycine (G)–histidine (H) and tryptophan (W)–aspartic acid (D) dipeptide repeats (2). They also happen to be incredibly abundant throughout the eukaryotic tree of life (3). Proteins with WD domains are primarily associated with signalosome assembly (4), providing the means for signal transduction, and there are as yet no WD domain proteins with intrinsic enzymatic capabilities (2). Besides signal transduction, WD domains are involved in processes ranging from organism proliferation to virulence in lower eukaryotes (5) or immune response in higher eukaryotes (1, 2, 6). RACK1 was indeed initially associated with protein kinase C signaling, the reason for its namesake (7). However, RACK1 is now known to have many, varying biological roles and functions with the primary role of RACK1 shown to be as a ribosomal protein (8–10). RACK1 has also been shown to be integral for multiple aspects of mRNA translation from efficient, cap-dependent mRNA translation initiation (8, 9, 11–14) to recruitment of factors necessary for multiple mRNA/ribosome-associated quality control pathways (15–19). The mammalian homolog is found to be stably associated with 40S ribosomal subunit and actively translating ribosomes, having an *in vitro* half-life of 15 h (8). This suggests a primary role of human RACK1 and its yeast ASC1 homolog as ribosomal proteins.

In *Plasmodium falciparum*, unlike yeast and mammalian cell lines (8), RACK1 is required for parasite growth during IDC stages, as knockdown during ring stage results in growth arrest in the trophozoite stage (20). Previous work has suggested that RACK1 is mainly localized to the parasitic cytoplasm during the schizont stage (20), but proteomic data has indicated that *P. falciparum* RACK1 (PfRACK1) might be exported to the erythrocyte cytoplasm for a yet to be define function (21). What remains unclear are the functions of RACK1 in the parasite, given the lack of a PKC IIβ homolog (14). Conflicting evidence has been provided regarding RACK1 ribosomal binding in *P. falciparum*. Structural data show that RACK1 does not copurify with schizont 80S ribosomes (22, 23), while mass spectrometry of polysome profiling data paints a contradictory picture (24). Authors of the initial structural study noted that loss of PfRACK1 binding to ribosomes may have been a result of different modes of ribosome binding or culturing conditions (22). Authors of the second structural study suggested that the loss of RACK1 interaction may be driven by stage-regulated binding, but not that of the EM sample preparation (23). The mass spectrometry data (24), however, indicated a primarily ribosome-bound RACK1 and suggested binding of RACK1 to the ribosome may be disrupted by experimental procedures. Lastly, the *in vitro* assessment of *P. falciparum* RACK1 ribosome binding was previously attempted with human ribosomes, however, authors were unable to exogenously produce and subsequently purify the parasite homolog due to suspected protein instability (8). As such, it is still unknown whether *P. falciparum*

* For correspondence: Sergej Djuranovic, sergej.djuranovic@wustl.edu.

RACK1 protein binds to ribosomes and whether this ribosomal binding is conserved like in the case of mammalian and yeast homologs.

Results

Sequence analysis of RACK1 proteins

As previously mentioned, RACK1 is a highly conserved, eukaryotic scaffolding protein with a seven-bladed WD β-propeller repeat structure (1). We performed bioinformatic analysis on a selected set of organisms including other single-celled parasitic organisms, a human malaria vector, the model organisms *Drosophila melanogaster, Saccharomyces cerevisiae*, and the human host (Fig. 1 and Table 1). Expectedly, the *Plasmodium* spp. shares the highest sequence identity with *P. falciparum* Dd2 strain RACK1 (PfRACK1) protein, whereby human-infective strains *Plasmodium vivax* P01 and *Plasmodium knowlesi* strain H show only minor differences. This is followed by the murine parasite species *Plasmodium chabaudi chabaudi, Plasmodium yoelii yoelii* 17X, and *Plasmodium berghei* ANKA. The RACK1 homolog expressed by *Toxoplasma gondii*, a fellow Apicomplexan whose genes and their functions are often compared with *P.* spp., is also quite similar at 67.30% (Table 1). Interestingly, the *Homo sapiens* RACK (HsRACK1) homolog has a shared identity of almost 60%, higher than other single-celled parasites (*Trypanosoma brucei*

brucei at 51.30% and *Leishmania brazilliensis* at 41.97%) and *S. cerevisiae* (ScRACK1, 42.99%) with which one might anticipate the parasite sharing greater sequence identity. Lastly, the model organism *D. melanogaster* and malaria vector *Anopheles gambiae* also share relatively high sequence identity at 58.15% and 56.45%, respectively.

Bioinformatic analysis of HsRACK1 and ScAsc1 proteins show that they share a 53.82% sequence identity, with HsRACK1 and PfRACK1 having higher sequence identity (59.55%). A multiple sequence alignment combined with secondary structure analysis of these RACK1 proteins was performed to further determine what features, if any, would affect the binding of PfRACK1 to the 40S ribosome subunit. The analysis demonstrates a conservation of the β-sheet blades and loop features and positioning (Fig. 2A).This is apparent in the overall structure of PfRACK1-generated model even in the regions that may have sequence variation and are indicated in the RACK1-ribosome binding regions (Fig. 2B, regions in blue and red). Previously described residues, such as the RDK motif vital to ribosome binding (Fig. 2A region 3 and Fig. 2C, DDE), are conserved with charge inversion by mutation of the arginine (R) to aspartate (D) and the lysine (K) to glutamate (E) resulting in the RDK→DDE mutation, which significantly reduces ribosome binding due to the increased negative charge of the amino acid triplicate clashing with that of the rRNA (1, 9, 10, 25). However, there are multiple regions within the

Figure 1. Clustal Omega alignment of RACK1 homolog protein sequences from selected organisms. The *Plasmodium falciparum* RACK1 protein sequence was aligned to selected organisms to compare with closely related, human-infective species (*Plasmodium vivax, Plasmodium knowlesi, Plasmodium reichenowi*) as well as murine model species (*Plasmodium berghei*). We also sought to examine conservation with the often compared parasite *Toxoplasma gondii* and other eukaryotic parasites (*Trypanosoma brucei, Leishmania brazilliensis*). Two model organisms, one unicellular (*Saccharomyces cerevisiae*) and the other multicellular (*Drosophila melanogaster*), were also included. Lastly, the human host (*Homo sapiens*) and vector (*Anopheles gambiae* PEST) were also examined, with the human host being a focal point of the analysis. Clustal Omega consensus symbols: Asterisks (*) indicates fully conserved residue. Colon (:) indicates conservation between residues of strongly similar properties (approximation of > 0.5 in the Gonnet PAM 250 matrix). Period (.) indicates conservation between residues of weakly similar properties (approximation of =< 0.5 and > 0 in the Gonnet PAM 250 matrix). RACK1, receptor for activated C-kinase 1.

Table 1

Analysis of RACK1 sequence identities *versus Plasmodium falciparum* Dd2 strain

Organism	Identity (%)
Plasmodium falciparum 3D7	100.00
Plasmodium reichenowi CDC	100.00
Plasmodium vivax P01	95.03
Plasmodium knowlesi strain H	95.03
Plasmodium chabaudi chabaudi	91.93
Plasmodium yoelii yoelii 17X	91.61
Plasmodium berghei ANKA	91.30
Toxoplasma gondii	67.30
Homo sapiens	59.55
Drosophila melanogaster	58.15
Anopheles gambiae PEST	56.45
Trypanosoma brucei brucei TREU927	51.30
Saccharomyces cerevisiae	42.99
Leishmania braziliensis MHOM/BR/75/M2904	41.97

Sequence identities were determined using protein BLAST to align protein sequences with *P. falciparum* Dd2 RACK1 protein sequence for each organism.

N-terminus whereby significant residue changes result in charges differences that could affect RACK1 ribosomal binding. Some of these changes have been subtle (Fig. 2, *A–C*, region 1), however, others are more drastic, such as changes in or introductions of charge Fig. 2, *A–C*, regions 2 and 5) or loop length and residue polarity (Fig. 2, *A–C*, region 4). The C-terminal of the proteins appear to be significantly more conserved with the exception of the so called "knob" region (Fig. 2, *A–C*, red) located in the sixth β-sheet blade suggested to be a species-specific region offering differences in translational control (26). This region was shown to be dispensable

in yeast (25). This sequence is encoded as FAGYS in yeast, STSS in humans, and KQS in *P. falciparum*. Regardless, previous work suggests that the loop region (Fig. 2, *A–C*, red) has evolved to accommodate differences in eIF6 binding and 5′ polyA leader sequence usage by different eukaryotic organisms, thereby not necessarily being important of ribosome binding (26).

Modeling of P. falciparum *RACK1 protein*

To get further insight into differences and similarities between PfRACK1 and HsRACK1 proteins, we created a *de novo* model of the PfRACK1 protein (Figs. 2 and 3). The model was generated based on the sequence alignments (Figs. 1 and 2) and homology modeling using SWISS-MODEL (27–31). This *de novo* model generated by SWISS-MODEL was also compared with the *P. falciparum* RACK1 model produced by the AlphaFold Protein Structure Database (32, 33), which showed no significant differences in the structure or ribosome interactions between the two models (Fig. S1). HsRACK1 has been previously shown to bind to the human 40S ribosome, with emphasis placed on helices 39 and 40 of the 18s rRNA and the N-terminal region of RACK1 (34). We checked whether this feature is preserved in *P. falciparum* RACK1 protein and displayed PfRACK1 as previously published for HsRACK1 interaction with the human 80S ribosome (34) (Fig. 3*A*). The helices 39 and 40 of the parasite 18S rRNA reveal the potential for highly similar
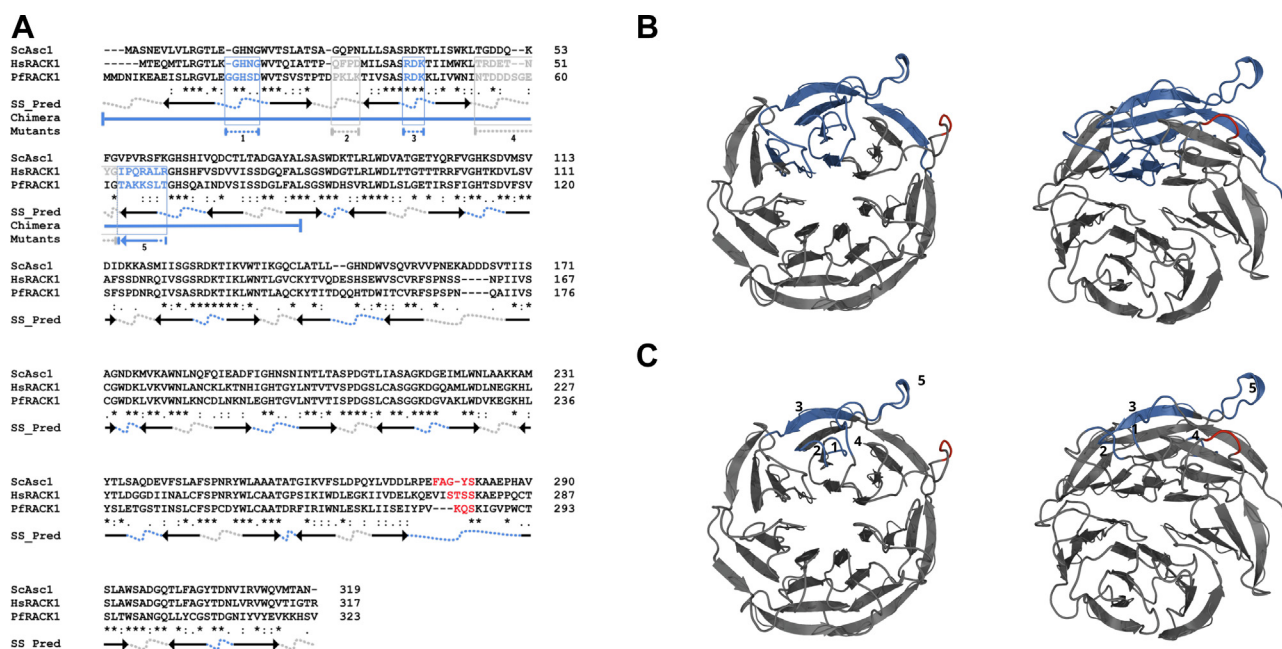

Figure 2. Comparative bioinformatic analysis of RACK1 homologs in *Saccharomyces cerevisiae* (ScAsc1), *Homo sapiens* (HsRACK1), and *Plasmodium falciparum* (PfRACK1) homologs. *A*, sequence alignment of yeast Asc1, human RACK1, and *Plasmodium falciparum* RACK1 amino acid sequences generated by Clustal Omega. The SS_Pred is the secondary structure prediction using MPI Bioinformatics toolkit Quick2D tool. *Arrows*: beta strands. *Arrows* represent beta strands, with heads pointing from the N-terminal to C-terminal direction showing the orientation of the beta strand in the β-propeller. *Dotted lines* represent loops found between beta strands where *gray* notates solvent-facing loops and *blue* indicates ribosome-facing loops. Chimera (χ): proteins generated by region exchanged between human and parasite RACK1 proteins shown in *solid blue lines*. RDK→DDE mutant is indicated in *blue text* and *blue dashed line*. Clustal Omega consensus symbols: *Asterisks* (*) indicates fully conserved residue. *Colon* (:) indicates conservation between residues of strongly similar properties (approximation of > 0.5 in the Gonnet PAM 250 matrix). *Period* (.) indicates conservation between residues of weakly similar properties (approximation of =< 0.5 and > 0 in the Gonnet PAM 250 matrix). *B* and *C*, a SWISS-MODEL generated *de novo* model of PfRACK1 displaying (*B*) chimeric region and (*C*) variable regions in *blue*. *Left*: Ribosome-facing surface. *Right*: 25-degree rotation. RACK1, receptor for activated C-kinase 1.
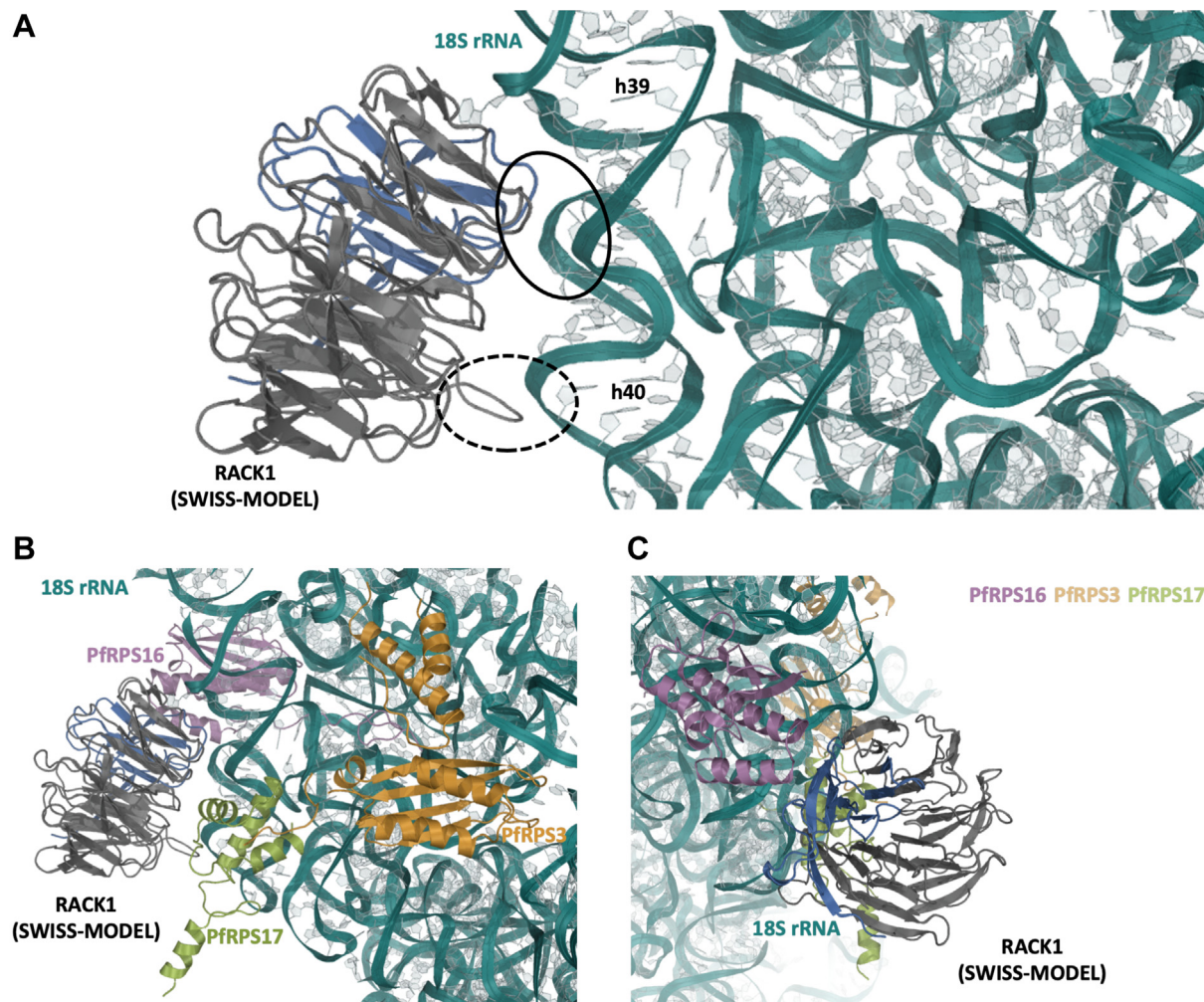
Figure 3. Structural analysis of the PfRACK1 protein binding to *Plasmodium falciparum* 40S ribosome subunit. All structures displayed are *Plasmodium falciparum* proteins/RNA. *A*, the structure of the *P. falciparum* 80S ribosome (RCSB PDB ID: 3jbo) was structurally aligned with the human 80S ribosome (RCSB PDB ID: 3jag). The *de novo* model of PfRACK1 generated by SWISS-MODEL was structurally aligned with that of the human 80S bound RACK1. The view shown is that which has been previously published arguing for the importance of the regions noted in RACK1 binding to the ribosome. *Solid circle*: region vital for HsRACK1:Hs80S binding. *Dotted circle*: Loop region that varies highly from species to species, and while not required, may influence binding. *B*, the same view as above, however, ribosomal-binding proteins with potential interactions are shown. *C*, a 180-degree flipped view to show additional RPS16 (uS9) and RACK1 interactions. Note: Region in *blue* is that when exchanged between human and *P. falciparum* enabled binding of parasite RACK1 to the human 40S ribosome. HsRACK1, *Homo sapiens* RACK1; PfRACK1, *Plasmodium falciparum* RACK1; RACK1, receptor for activated C-kinase 1.

interactions between the PfRACK1 protein and the *P. falciparum* 18S rRNA. Previous work also examined ribosomal proteins in this region: RPS16 (uS9), RPS17 (eS17), and RPS3 (uS3) (Fig. 3, *B* and *C*), which are also in close proximity. Therefore, residues that may interact with these proteins must also be taken into consideration. Those residues on PfRPS16 and PfRPS17 within 3 to 5 Å range are also highly conserved (Fig. S2) and therefore are not expected to hinder binding. The residues of PfRPS3 are also highly conserved, however, it appears that there may be a C-terminal truncation of 18 residues when compared with HsRPS3 that may impact interaction of the disordered region of the protein (Fig. S2). Overall, the PfRACK1 model data shows high sequence and structural conservation of the PfRACK1 protein compared with HsRACK1 and indicating the possibility of for PfRACK1 to bind the ribosome.

PfRACK1 expression follows other ribosomal proteins

We performed transcriptional analysis of PfRACK1 to compare its expression profile over the different parasite life stages as well as correlation with expression of *P. falciparum* ribosomal proteins. RNAseq data for all available *P. falciparum* proteins for the ring, early trophozoite, late trophozoite, schizont, gametocyte II, gametocyte V, ookinete, oocyst, and sporozoite stages from the previous study (35) were collected from PlasmoDB (36). A violin plot (Fig. 4*A*, solid) of all data, other than PfRACK1 and ribosomal proteins, was generated. The ribosomal proteins were plotted as another violin plot (Fig. 4*A*, dotted outline). The RNAseq data points for RACK1 were then plotted (Fig. 4*A*, dot plot) to compare the RNA expression of RACK1 with the ribosomal proteins *versus* all parasite proteins. Our analysis shows that the PfRACK1 gene, like other ribosomal proteins, is highly expressed in

comparison to the average total protein transcript expression at each stage and in a pattern similar to other ribosomal proteins (Fig. 4*A*). Notably, PfRACK1 expression drops by approximately one $\log_{10}$ from the early trophozoite stage where translation is high to when the parasites transition into the schizont stage. A pairwise *t* test was performed on the three groups and further suggested that PfRACK1 RNA expression is more closely aligned to that of ribosomal proteins than nonribosomal proteins (Table S1). However, a normal Q-Q plot of the data indicated a non-normal distribution (Fig. S3). Therefore, a pairwise Wilcox test was done, which again suggested that PfRACK1 RNA expression is more closely aligned to that of ribosomal proteins than nonribosomal proteins; however, with more statistical significance (Table S2). Thus, the RNAseq data suggests that PfRACK expression follows that of other ribosomal proteins and significant changes in expression are seen during stages where protein synthesis dramatically increases or decreases.

Analysis of the protein mass spectrometry data was also performed. Protein mass spectrometry data for all available *P. falciparum* proteins for the ring, trophozoite, and schizont stages of a previous study (37) was collected from PlasmoDB (36). A pairwise *t* test of the data revealed that no differences in the three groups exist (Table S3). Again, a normal Q-Q plot of the data suggests that while most of the data falls within the normal distributions, the dataset may have a non-normal distribution (Fig. S4) and a pairwise Wilcox test was also performed and again indicated that no differences in the three groups exist (Table S4). However, it should be noted that protein mass spectrometry data is not available for many parasite proteins, with only about a third of proteins having data, which could dramatically alter the analysis (Fig. 4*B*).

Expression of chimeric and mutant RACK1 proteins

To compare ribosomal binding of human and *P. falciparum* RACK1, WT, chimeric, and mutant constructs were generated

based on bioinformatic and structural model analyses (Figs. 2, *A*–*C*, 3, and 5*A*), as well as previous work (1, 8–10, 25). While most of the ribosome-facing loop residues appear conserved, previous work has shown that small single or double amino acid changes in key regions are able to significantly change binding (1, 9, 10, 25), thus the RDK→DDE mutation was included as a control to show any potential reduction of binding (Fig. 2, *A* and *C* region 3, and Fig. 5*A*). Previous work also emphasized the importance of the N-terminal region in RACK1 binding to the human 40S ribosomal subunit (1). As such, we generated chimeric RACK1 variants by exchanging the N-terminal regions of HsRACK1 (residues 1–79) and PfRACK1 (residues 1–88). Multiple regions in the N-terminus of RACK1 differ between human and *P. falciparum* that could potentially influence binding to ribosomes. Some alterations appear subtle, such as the introduction of a negatively charged aspartate, which may reduce interaction with the negatively charged rRNA backbone (Fig. 2, *A* and *C* region 1). The other differences appear more drastic in the sequence of PfRACK1 protein, incorporating significant amounts of positively or negatively charged residue in contrast to the human homolog (Fig. 2, *A* and *C*, regions 2, 4, 5). It is important to note that the *P. falciparum* homolog is encoded using a significant number of rare human codons and therefore codon optimization using the Java Codon Adaptation Tool Available at: jcat.de was necessary for expression in mammalian cell lines. These constructs were expressed in HAP1 ΔRACK1 cells (38) and *P. falciparum* Dd2 parasites (Fig. 5). RACK1 constructs with an N-terminal flag tag were transduced by lentivirus into HAP1 ΔRACK1 cells (Fig. 5*B*). RACK1 was C-terminally tagged with fluorescent mNeonGreen followed by a 3x hemagglutinin affinity tag and electroporated into *P. falciparum* Dd2 cells (Fig. 5*C*). Western blot analysis of human and parasite RACK1 lines indicates single band at ~37 kDa for expression in human HAP1 cells and an ~65 kDa band for expression in *P. falciparum* cells. The WT proteins showed similar
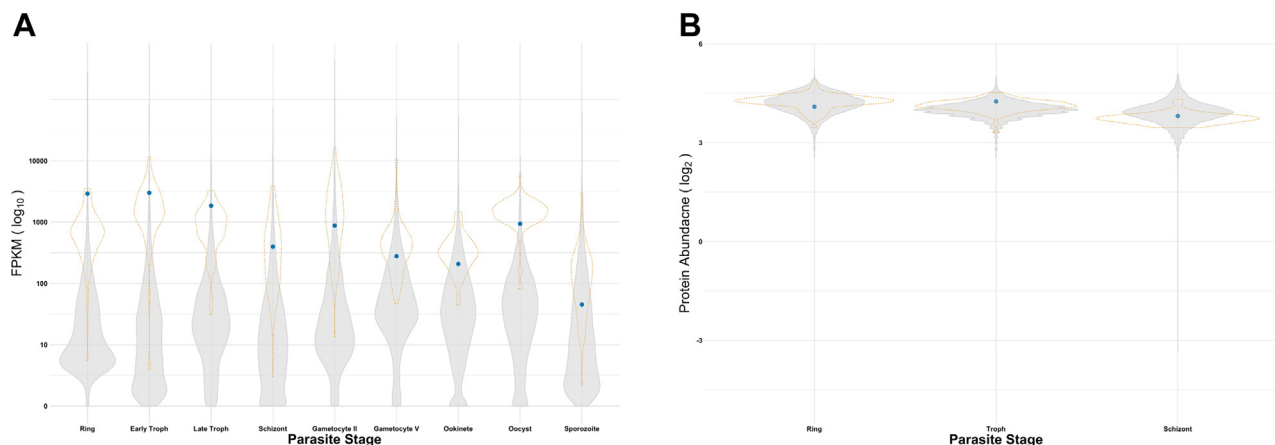
Figure 4. Transcriptional analysis of PfRACK1 in comparison with other parasite protein-coding genes throughout the *Plasmodium falciparum* life cycle. *A*, RNASeq data from PlasmoDB showing all protein-coding genes (*solid violin plot*), ribosomal protein (*dotted violin plot*), and PfRACK1 (*blue dot*) transcript expression in *Plasmodium falciparum* 3D7 throughout the parasite life cycle. The x-axis indicates the parasite stage and the y-axis ($\log_{10}$ scale) represents transcript fragments per kilobase of exon model per million reads mapped. *B*, protein mass spectrometry from PlasmoDB showing all proteins (*solid violin plot*), ribosomal protein (*dotted violin plot*), and PfRACK1 (*blue dot*) protein abundance in *P. falciparum* 3D7 throughout the parasite life cycle. The x-axis indicates the parasite stage and the y-axis ($\log_{2}$ scale) represents abundance of protein. PfRACK1, *Plasmodium falciparum* RACK1; RACK1, receptor for activated C-kinase 1.
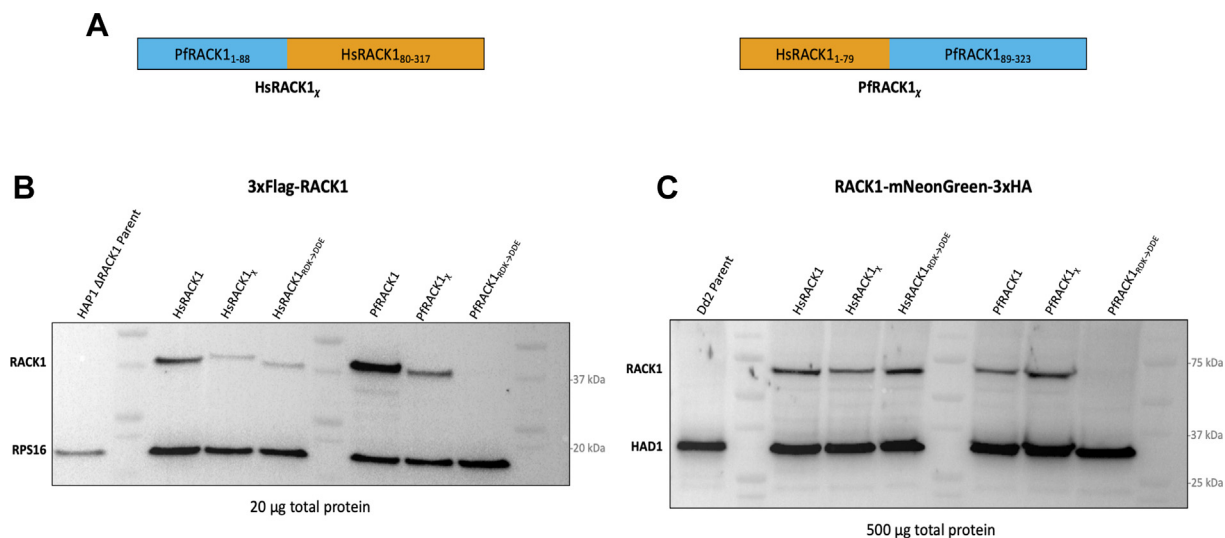
Figure 5. Expression of RACK1 variants in mammalian HAP1 ΔRACK1 cells and P. falciparum parasites. *A*, schematic constructs for RACK1 variants. HsRACK1$_\chi$ designates the RACK1 chimera comprised of an N-terminus with PfRACK1 amino acids 1 to 88 followed by a C-terminus with HsRACK1 residues 80 to 317 (*left*). PfRACK1$_\chi$ designates the RACK1 chimera comprised of an N-terminus with HsRACK1 amino acids 1 to 79 followed by a C-terminus with PfRACK1 residues 89 to 323 (*right*). HsRACK1$_{RDK\rightarrow DDE}$ and PfRACK1$_{RDK\rightarrow DDE}$ constructs generated by mutating HsRACK1 Arg$_{36}$/Lys$_{38}$ or PfRACK1 Arg$_{43}$/Lys$_{45}$ to Asp/Glu. *B*, Western blot using anti-Flag antibody of HAP1 ΔRACK1 cell expressing RACK1 variants. 40S ribosomal protein 16 (uS9) blotted as control. *C*, Western blot using anti-HA antibody of *Plasmodium falciparum* parasites expressing RACK1 variants. Haloacid dehalogenase-like hydrolase (HAD) blotted as control. HsRACK1, *Homo sapiens* RACK1; PfRACK1, *Plasmodium falciparum* RACK1; RACK1, receptor for activated C-kinase 1.

expression in both HAP1 and parasite cells (Fig. 5, *B* and *C*). Mutants and chimeric proteins varied in their expression (Figs. 5, *B* and *C*, S5). The patterns also differed between human and parasite cells. The constant between the two organisms was that the RDK→DDE mutant was anticipated to have significantly impaired binding in both organisms given the sequence conservation and its importance in previous work (1, 9, 10, 25). RACK1, like other ribosomal proteins (39), is unstable when not bound to the ribosome (9) and this, along with potential issues of folding, may account for the reduction in protein of some constructs.

Localization of RACK1 protein in P. falciparum *cells*

Previous work has stated that in *P. falciparum*, RACK1 is dispersed in the parasite cytoplasm during the schizont stage and it might be exported into the red blood cell (21), the stage from which all previous ribosome structural data is based (22, 23). To reevaluate this phenomenon, live imaging microscopy was performed on *P. falciparum* Dd2 lines expressing C-terminally tagged mNeonGreen WT PfRACK. The developmentally mixed culture of parasites was treated with E64 to obtain late-stage schizonts. Hoechst 33342 stain (blue) was used to stain parasite DNA while BODIPY TR ceramide (red) was used to label host/parasite membrane, and mNeonGreen (green) was used to tag the exogenously expressed parasite RACK1 protein. Images were taken of the Dd2 parent line (Fig. 6*A*) and Dd2 expressing mNeonGreen-tagged PfRACK1 (Fig. 6*B*) in both trophozoite and schizont stages of development. BODIPY TR ceramide staining shows parasite daughter cells labeled within the host RBC while PfRACK1 mNeon-Green signal maintains close contact within these daughter cells showing no staining in the RBC cytoplasm. Therefore, imaging of schizonts did not show dispersal of RACK1 into the

red blood cell cytoplasm but rather the RACK1 protein remains in the parasite cytoplasm surrounding the daughter cells as seen previously (20).

Ribosome association of RACK1 chimeras and variants

To assess the binding of RACK1 to human and *P. falciparum* ribosomes and 40S subunits, we isolated crude ribosomes by running cell lysates through a sucrose cushion and then examined the presence of RACK1 in the crude ribosome pellet. We used the small ribosomal subunit protein 16 (RPS16) to follow pelleted ribosomes. The RACK1 variants expressed in HAP1 cells harboring the human RACK1 N-terminal region were able to bind the human ribosome while those that had the parasite RACK1 N-terminal region did not show significant binding to human ribosomes (Fig. 7*A*) when compared to RPS16 pelleted amounts. This difference in ribosome binding and potential association is most prominent between HsRACK1 and HsRACK1χ chimera as well as between PfRACK1 and PfRACK1χ chimera. HsRACK1 and PfRACK1χ chimera (human N-terminal region) were detected more in ribosome pelleted fraction than in the human cell lysate, similar to RPS16. PfRACK1 and HsRACK1χ chimera (*P. falciparum* N-terminal region) in contrast had the opposite distribution with more protein detected in lysates than in ribosomal pellets, contrary to RPS16 (Fig. 7*A*). The loss of binding to human ribosomes was observed for the RDK→DDE mutation as in previous studies (1, 8, 11, 25) (Fig. 7*A*). Interestingly, all variants appeared to bind in *P. falciparum* parasite, potentially even the poorly expressed PfRACK1 RDK→DDE mutant, suggesting a difference in RACK1::40S subunit binding in the parasite (Fig. 7*B*). Furthermore, Western blot analysis of ribosomal fractions collected during polysome profiling in parasites suggest that PfRACK1 is bound to the ribosome
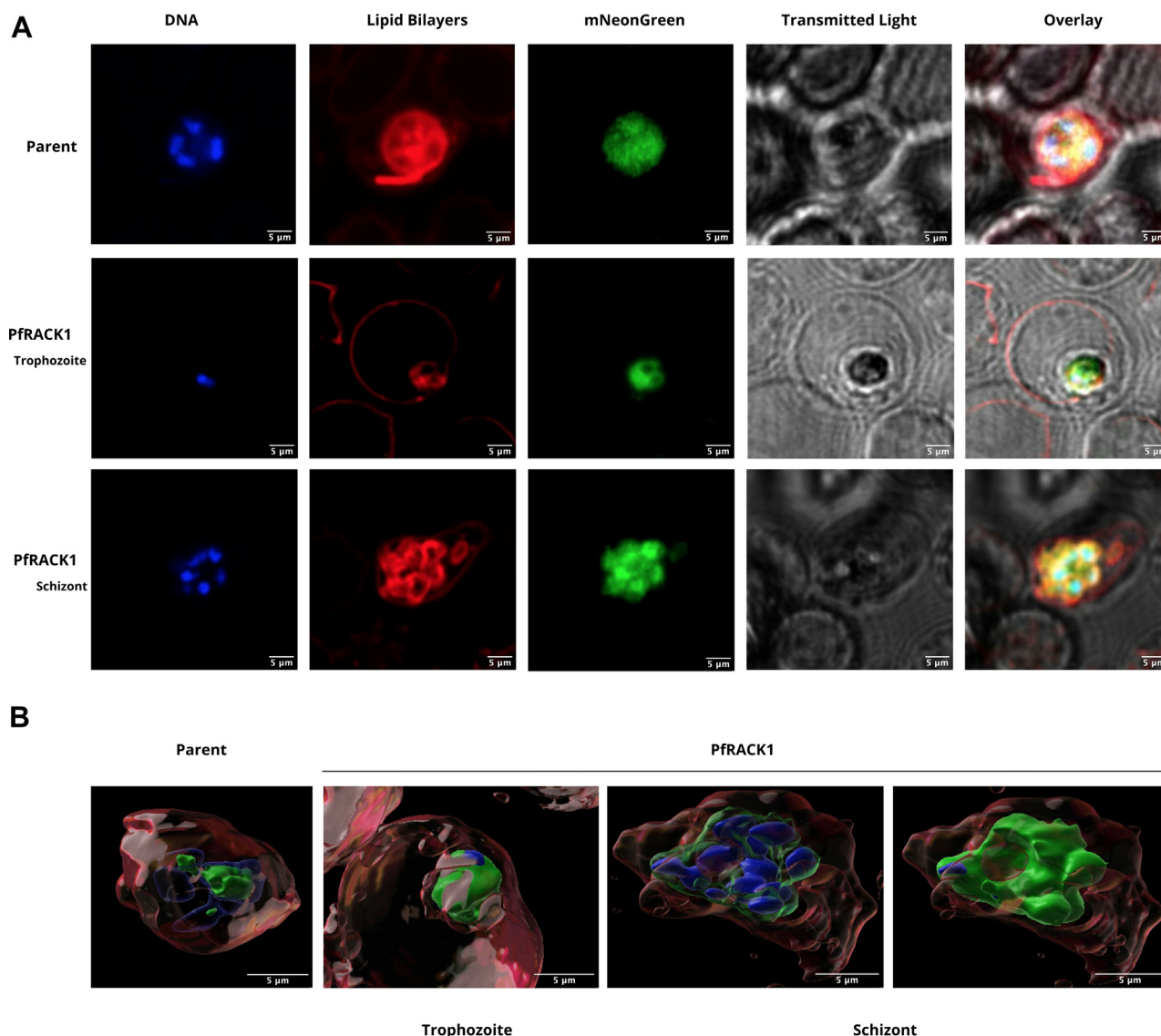
Figure 6. Airyscan confocal fluorescence imaging microscopy of mNeonGreen-tagged PfRACK1 expressed in *Plasmodium falciparum*. *A*, Hoechst stain (DNA), BODIPY TR ceramide (lipid bilayers), mNeonGreen (RACK1), transmitted-photomultiplier tube (T-PMT) as brightfield, and overlay images. *Top*: Dd2 parent line. *Middle*: Dd2 parent line expressing mNeonGreen-tagged PfRACK1 at trophozoite stage. *Bottom*: Dd2 parent line expressing mNeonGreen-tagged PfRACK1 at schizont stage. *B*, two-dimensional overlay using Imaris software analysis of Airyscan images. *Left*: Dd2 parent line at the schizont stage. *Right*: Dd2 parent line expressing mNeonGreen-tagged PfRACK1 in trophozoite and schizont stages. The size bar in the images represents 5 µM. PfRACK1, *Plasmodium falciparum* RACK1; RACK1, receptor for activated C-kinase 1.

during translation similar like HsRACK1 and chimeric proteins (Fig. S6). Finally, the ribosome binding of RACK1 variants (Fig. 7B) was also seen by RT-qPCR analyses of rRNAs bound to the immune-precipitated RACK1 protein variants (Fig. S7). Immunoprecipitation of all RACK1 variants and chimeras, except PfRACK1 RDK→DDE mutant, resulted in enrichment of bound rRNAs in RT-qPCR analysis (Fig. S7) albeit with different ratios for 40S and 60S subunits. As such, our data suggests that in comparison to the human RACK1 protein, PfRACK1 binds specifically to the parasite ribosomes with little, if any, affinity toward human ribosomes.

Discussion

With an approximately 60% shared sequence identity between the human and *P. falciparum* RACK1 proteins, sequence and structural analysis reveal that PfRACK1 maintains all the hallmark characteristics of homologs where ribosomal binding is seen (Figs. 1–3). This is particularly true of ribosomes facing residues. Combining the sequence analysis data with the *de novo* structure of PfRACK1 modeled onto the parasite 80S ribosome, most of the ribosome-facing loop residues appear conserved in nature and similar to human RACK1 protein (Figs. 2 and 3). Additionally, the potential rRNA interactions also appear to be conserved in the parasite, as do those of RPS16 (uS9), RPS17 (eS17), and RPS3 (uS3) with the exception of a potential alteration to the RPS3 C-terminal disordered region (Fig. S2). Bioinformatics analysis of PfRACK1 (20, 40) mRNA abundance demonstrates that the transcriptional profile of PfRACK1 mRNA follows other ribosomal proteins (Fig. 4A, Tables S1 and S2) further enabling its role in protein synthesis. However, not enough mass
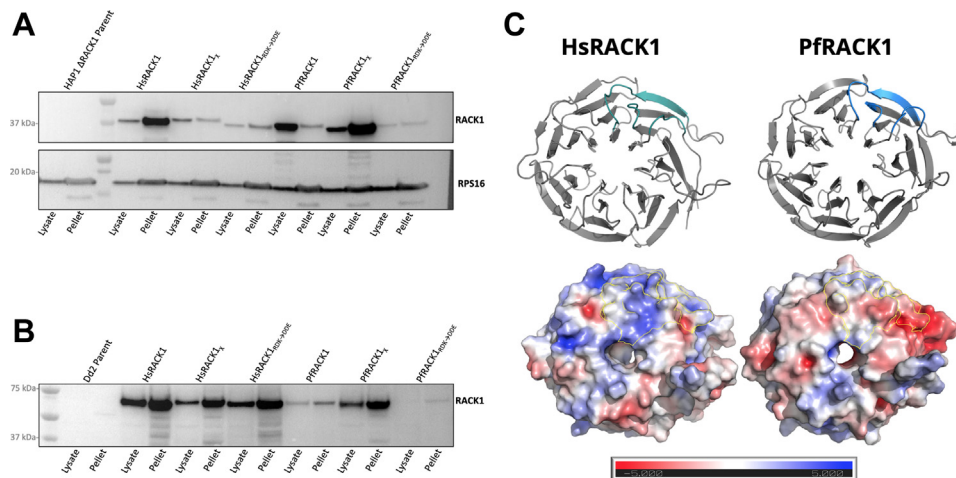
Figure 7. Ribosomal binding of RACK1 variants in mammalian HAP1 ΔRACK1 cells and *Plasmodium falciparum* parasites. *A*, Western blot of lysates and postsucrose cushion centrifugation pellets of HAP1 ΔRACK1 cells expressing N-terminally 3xFlag tagged RACK1 variants. 40S ribosomal protein 16 (uS9) blotted as control. *B*, Western blot of lysates and postsucrose cushion centrifugation pellets from *Plasmodium falciparum* parasites expressing C-terminally 3xHA-tagged RACK1 variants. *C*, ribbon model (*above*) displays ribosome-facing structure with colored region indicating N-terminal section previously shown to be important for binding in mammalian cells. Electrostatic map (*below*) of above ribbon model ribosome-facing surface for human and *P. falciparum* RACK1 proteins generated using PyMOL APBS Electrostatics plugin. *Outlines* indicate colored region of N-terminal section previously shown to be important for RACK1 binding in mammalian cells. RACK1, receptor for activated C-kinase 1.

spectrometry data is available for a definitive analysis of the protein behavior (Fig. 4B, Tables S3 and S4). Regardless, taken together, this data as well as previous studies on yeast and mammalian RACK1 homologs suggested that PfRACK1 should be able to bind to the parasite 40S ribosomal subunit.

To examine PfRACK1 binding of the 40S ribosome subunit, we generated RACK1 variants based on bioinformatic and structural analysis. We also generated chimeras between human and *P. falciparum* RACK1 proteins, switching N-terminal regions. Expression of the WT HsRACK1 and PfRACK1 appeared to be comparable within HAP1 ΔRACK1 mammalian cells (38) and *P. falciparum* parasites (Fig. 5, *B* and *C*). In parasite lines, expression of all variants appeared approximately equal with exception of the PfRACK1$_{RDK \to DDE}$ mutant that is expected to have reduced ribosome binding and reduced stability (1, 8, 11, 25). In the mammalian line, both human and *P. falciparum* RACK1$_{RDK \to DDE}$ mutants as well as RACK1 chimera with N-terminal region from *P. falciparum* (HsRACK1χ) showed reduced expression. It has been shown that, like most ribosomal proteins (39), RACK1 becomes unstable when not bound to the ribosome (9), which may explain the lower expression levels and predict subsequent ribosome binding in that organism. In this respect, those RACK1 variants that contained the *P. falciparum* N-terminal region as well as those with the RDK→DDE mutation might have reduced stability arguing for some differences and specificity in RACK1 binding in *P. falciparum* cells.

Since it was previously suggested that PfRACK1 is exported during the schizont stage into the red blood cell cytoplasm (21), we tagged PfRACK1 with the fluorescent reporter mNeonGreen. To enrich for parasites during the schizont stage, parasites were treated with E64, which prevents RBC membrane rupture (41, 42). Parasites were subsequently examined by confocal microscopy with airyscan to determine PfRACK1 localization in relation to parasite DNA and lipid

bilayers. We did not find confirmation for the previously observed phenomenon of PfRACK1 export (21) but rather that of the localization and dispersion of PfRACK1 in the parasitic cytoplasm (20). Our data indicated that mNeonGreen-tagged PfRACK1 remained within the schizont cytoplasm (Fig. 6). While our data suggests that PfRACK1 is found within the parasite during the schizont stage, it is possible that the parasites were not incubated long enough to see release of the protein into the RBC cytoplasm. However, the phenomenon of exported PfRACK1 protein is most likely due to the perforation of the parasitophorous vacuole that occurs at late in this stage (43).

Finally, our data indicates that *P. falciparum* RACK1 protein may have a different mode of binding to parasite ribosomes (Fig. 7C). Previous studies reported that yeast RACK1 homolog Asc1 (ScAsc1) has been shown to be able to bind the human 40S ribosome subunit (8). Although PfRACK1 shares a higher identity with HsRACK1 than ScAsc1 (59.55% *versus* 53.82%), it was unable to bind the human ribosome (Fig. 7A). Analysis of ribosome binding in the parasite cells, however, shows that not only does PfRACK1 bind the ribosome (Figs. 7B, S5 and S6) but also that binding is altered from that of human ribosomes (Figs. 7B, S5 and S6), with less emphasis on N-terminus driven binding in parasite. Polysome profiling data also show that PfRACK1 is indeed found in the 80S and polysome fractions (Figs. S6 and S7), but there is a reduction in the presence of PfRACK1 in this fraction compared to the HsRACK1 and PfRACK1$_X$ variants when assayed in parasite cells. This again suggests an alteration in PfRACK1 binding of the 40S subunit and species-specific interactions (9–11, 26, 34). Using the previously generated cryoEM structure of HsRACK1 and our *de novo* model of PfRACK1, we modeled the electrostatic composition of the ribosome-facing surface of RACK1 for human and *P. falciparum* (Fig. 7C). The comparison shows a dramatic difference in the charge distribution between the two

organisms, particularly in the N-terminal region thought to be most important for binding of RACK1 protein to rRNA in humans (Fig. 7*C*, outlined region). This once again suggests a difference in mode of RACK1 binding in parasites *versus* the human host. However, this data does not include any post-translational modifications that could further alter ribosome binding of RACK1 in parasite nor any specific contacts with disordered regions of ribosomal proteins.

According to currently available structural data, RACK1 does not copurify with schizont 80S ribosomes (22, 23). This may be the result of purification method artifacts (44), such as the loss of polysomes with use of saponin lysis (45). The presence of RACK1 on the ribosome seen in crude ribosomes and polysome profiling data here (Figs. 7*B*, S5 and S6) and from others (46) indicate that PfRACK1 does indeed bind the ribosome. The interaction of PfRACK1 and ribosomes might be loose and could potentially explain that in cryoEM data (22, 23) PfRACK1 is not bound to a substantial portion of the particles used for the reconstruction of the ribosome structure. Our data on pull-down of *P. falciparum* rRNAs by RACK1 variants (Fig. S7) indicate possibility of such scenario. Tagged PfRACK1 protein is able to pull down ribosomal subunits but with different ratio of 40S and 60S subunits and decrease in overall ribosome amount compared to HsRACK1 variants or chimera with human N-terminal part of RACK1 protein (PfRACK1$_{\chi}$). This again may indicate different binding affinities of the N-terminal part of RACK1 proteins from human and possible *P. falciparum* species-specific RACK1 interactions (9–11, 26, 34). This does not also exclude the possibility of a change in PfRACK1::40S ribosome binding dynamics during the schizont stage (23). It is important to note that there is an almost $\log_{10}$ reduction in PfRACK1 transcript expression in the schizont stage (Fig. 4). One could hypothesize that the drastic reduction of PfRACK1 expression and ribosome binding, which has previously been shown to globally downregulate mRNA translation (9), would be energetically favorable as the parasite prepares to release short-lived and translationally less active merozoites.

Conclusion

Here, we demonstrate that RACK1 expression in *P. falciparum* follows that of other ribosomal proteins, binds to the parasite ribosome, and is present during active translation. Our data also shows that the RACK1::40S binding dynamics are quite different between mammalian and parasites, with emphasis on binding being distributed throughout the protein or even on the C-terminal region; potentially the loop motif. Finally, PfRACK1 is also localized to the parasite cytoplasm during the schizont stage in sharp contrast to the previously published work.

Experimental procedures

Transcriptional, bioinformatic, and structural analysis of P. falciparum RACK1

In order to analyze expression of *P. falciparum* RACK1 protein and potential interaction with ribosomes, we extracted transcriptional data for all ribosomal proteins from PlasmoDB (36), excluding apicoplast and mitochondrial genes. Ribosomal proteins during the human stage were defined as those with RNAseq expression data in the minimum of the 80th percentile during ring, early trophozoite, late trophozoite, schizont, gametocyte II, or gametocyte V[35] or during sporozoite stage (47). Ribosomal proteins expressed during the mosquito stage were defined as those with RNAseq expression data in the minimum of the 80th percentile during ookinete (35), oocyst, or sporozoite stage (47).

Sequence analysis of RACK1 and ribosomal protein amino acid sequences was done by alignment using the Clustal Omega multiple sequence alignment tool (48). The NCBI blastp suit was used to perform pair-wise sequence identity analysis on RACK1 amino acid sequences (49, 50). The secondary structure prediction was performed using the Quick2D tool in the MPI Bioinformatics Toolkit (51–57). All structural alignments were performed using PyMOL (Version 2.0 Schrödinger, LLC; http://www.pymol.org/pymol). The resulting *de novo* PfRACK1 model was added to the previously generated *P. falciparum* 80S structure (3JBO) (23). First, the *de novo* PfRACK1 model was structurally aligned to the human RACK1 protein found in the previously generated *H. sapiens* 80S structure (3JAG) (58). The *P. falciparum* 80S structure was then structurally aligned to the *H. sapiens* 80S structure, leaving only *P. falciparum* 80S structure in the figure. Interacting residues between the 80S ribosome and RACK1 protein were those found to be within a 3 to 5 Å range. Electrostatic maps were generated using PyMOL APBS Electrostatics plugin (59).

De novo *modeling of* P. falciparum *RACK1*

The RACK1 variants were modeled using SWISS-MODEL (27–31). Briefly, the RACK1 variant amino acid sequences were entered into the SWISS-MODEL server. The SWISS-MODEL software generates a list of potential structural templates based on the input. The software then aligns and models the input RACK1 variants on the selected templates and subsequently evaluates the quality of the model. Templates are then selected initially based on the GMQE score, coverage, and resolution. A final template is then selected based on the QMEAN score. Here, all RACK1 variants aligned and modeled well with the 4aow.1.A template, an X-ray crystallography generated structure of human RACK1 (48). For comparison, *de novo* structures were also collected from the AlphaFold Protein Structure Database (32, 33).

RACK1 variant construction

The PfRACK1 gene was codon optimized for expression in human cells. The HsRACK1 gene was cloned from cDNA. None of the expressed RACK1 variants have the typical intron that appears to be conserved in the gene. Based on bioinformatic and structural analysis, RACK1 variants were designed. The swapping of the N-terminal regions and other mutants were generated by mutagenesis PCR, whereby the 5′ and 3′ PCR products were produced overlapping in the

mutated regions. These products were combined by stitching PCR and cloned into the desired expression vectors. Clones of vectors with RACK1 variants were confirmed by Sanger sequencing.

Mammalian cell culture, lentivirus production, and transduction

Human embryonic kidney (HEK) 293T cells were cultured in Dulbecco's modified Eagle's medium (DMEM) (Gibco) and supplemented with 10% (v/v) fetal bovine serum, 5% (w/v) penicillin and streptomycin (Gibco), and L-glutamine (Gibco). HAP1 cells were cultured in Iscove's Modified Dulbecco's Medium (Gibco) and supplemented with 10% (v/v) Fetalgro Bovine Growth Serum (RMBIO), 5% (w/v) penicillin and streptomycin (Gibco), and L-glutamine (Gibco). Cells were grown at 37 °C with 5% CO_2. HAP1 ΔRACK1 cell lines previously generated ([38]) were obtained from source authors.

Tools for lentiviral production were generously provided by the You Lab (Washington University). The RACK1 variants to be expressed were cloned into the pCDH vector using the XbaI and NotI restriction sites and confirmed by Sanger sequencing. Plasmid DNA from pCDH-RACK1, pCMV-VSVG vector (addgene 8454), and psPAX2 vector (Addgene 12260) was isolated from bacterial midipreps (Invitrogen). Before transfection (20–24 h), 1.5 million HEK 293T cells were added in a 6 cm dish. The packaging vectors, pCMV-VSVG and psPAX2, were combined in a ratio of 1:9. For transfection, 3 μg of expression vector and 3 μg of combined packaging vectors were also combined in 400 μl of OPTI-MEM (Gibco). To this, 18 μl (1:3 ratio of DNA to transfection reagent) of X-treme-eGENE 9 DNA transfection reagent (MilliPore Sigma) was added. The mixture was incubated for 30 min at room temperature. The medium of HEK 293T cells was replaced with prewarmed regular growth medium. The transfection mixture was added, and the cells were put back in the incubator at 37 °C with 5% CO_2. On the next day, 1 ml of fetal bovine serum was added. The medium containing virus was collected at 48 h and 72 h after transfection. The supernatant containing the virus was centrifuged at 15,000g and then filtered using 0.45 μm filter to remove any 293T cells or debris. The virus was stored at 4 °C for up to 1 week or kept at –80 °C for long term storage and freeze-thawing avoided.

For lentiviral transduction, HAP1 cells were seeded such that they will be about 60 to 70% confluent at the time of transduction. To assess viral titer, cells were plated in 12-well plates. However, a 1:4 dilution was found to be sufficient enough for an almost 100% transduction. At 20 to 24 h after plating, polybrene was added to a final concentration of 8 μg/ml to cells, and the desired amount of lentivirus was added. At 48 h after transduction, cells were replated and selected with 3 μg/ml puromycin for 24 h, two to three times.

Parasite cell culture and transfection

P. falciparum Dd2 was cultured at 2 to 5% hematocrit in O$^+$ erythrocytes in Malaria Culture Medium: RPMI 1640 supplemented with 5 g/L Albumax II (Gibco), 0.12 mM

hypoxanthine (1.2 ml 0.1 M hypoxanthine in 1 M NaOH), and 10 μg/ml gentamicin ([60]). Cultures were grown statically in candle jar atmosphere. As required, cultures were synchronized with 5% (w/v) sorbitol. Asynchronous *P. falciparum* Dd2 parasites were washed twice in 15 ml incomplete Cytomix (25 mM Hepes, 0.15 mM $CaCl_2$, 5 mM $MgCl_2$, 2 mM EGTA, 120 mM KCl, 5 mM K_2HPO_4, 5 mM KH_2PO_4) and resuspended in a total 525 μl with 100 μg of maxi-prep plasmid DNA dissolved in incomplete cytomix (125 μl packed infected red blood cells (iRBCs) and 400 μl DNA/incomplete cytomix). The parasites were transfected in Bio-Rad Gene Pulser cuvette (0.2 cm), 0.31 kV, 950 up, infinity resistance. Selection (10 nM WR99210 or 2 μM DSM-1) was added to parasite 48 h after transfection and used to select resistant parasites ([61]). The DNA was isolated from the selected parasite cultures and each cell culture was genotyped for the presence of engineered version of RACK1 variants using PCR genotyping (Fig. S8) and subsequent Sanger sequencing (Table S5). The rDNA from genomic DNA was used as a control by amplification of 18S rRNA locus (151 bp) by 18S rRNA specific qPCR primers (Fig. S8 and Table S6).

Saponin lysis of iRBCs

The cell iRBCs were resuspended in two volumes of PBS containing 0.15% (w/v) saponin and incubated on ice for 10 min, with vigorous mixing every 3 min. Afterward, the samples were centrifuged 7000g, for 5 min at 4 °C, and the pellets were washed three times more with the same buffer.

Parasite staining and confocal microscopy with airyscan

To examine localization of RACK1 variants in the parasite, confocal microscopy using the Zeiss LSM 880 Confocal with Airyscan was performed. Primarily late trophozoite, early schizont stage parasites were treated for 6 h with E64 to inhibit parasite release ([41], [42]). Parasites were then washed twice using parasite imaging medium (RPMI without phenol red and with hypoxanthine) containing E64. Parasites were incubated for 30 min with Hoechst stain to label DNA and BODIPY TR ceramide to label lipids. Parasites were again washed 3 times with imaging medium containing E64. Cultures were dotted onto slides and sealed beneath coverslips. Transmitted-photomultiplier tube was used for brightfield images, and z-stacks were collected using a Zeiss LSM 880 Confocal with Airyscan confocal microscope using a 40X oil objective. DNA was visualized by Hoechst stain (diode: 405 nm, ex: 350 nm, em: 461 nm), RACK by mNeonGreen (laser: 488 nm, ex: 506, em: 517), and lipid bilayers by BODIPY TR ceramide (laser: 561 nm, ex:589/em:617). Image analysis and generation were done using Imaris (Oxford Instruments) and Fiji ImageJ software.

Crude ribosome preparation and polysome profiling

Crude ribosome pellets and polysome profiling in *P. falciparum* cells was done based on previous work ([24]). Parasites were grown to 7 to 10% parasitemia in 1.5 to 2.0 ml of packed iRBCs. Parasites were treated with culture medium

containing 200 μM cyclohexamide (CHX) for 10 min at 37 °C. They were then washed three times with 1X PBS + 200 μM CHX. Samples were then flash-frozen in liquid nitrogen and stored at –80 °C overnight. To the frozen samples, two volumes of lysis buffer (25 mM potassium Hepes pH 7.2, 400 mM potassium acetate, 15 mM magnesium acetate, 1% (v/v) IGEPAL CA-360, 200 μM CHX, 1 mM DTT, 1 mM AEBSF, 40 U/ml RNase inhibitor) and 0.5 mg of acid washed glass beads (Sigma #G8772) were added. Samples were rotated end-over-end at 4 °C for 10 min. Samples were centrifugated for 5 min at 1000*g*. Supernatants were transferred to a new tube and centrifugated at 14000*g* for 10 min. The supernatant was layered over 1 M sucrose cushion (1 M sucrose, 25 mM potassium Hepes pH 7.2, 400 mM potassium acetate, 15 mM magnesium acetate, 200 μM CHX, 1 mM DTT, 1 mM AEBSF, 40 U/ml RNase inhibitor) in a ratio of 2 ml lysate to 1 ml sucrose cushion. The balanced tubes were then placed in a TLA 100.3 rotor and centrifuged for 30 min at 335,000*g* at 4 °C using an Optima Max-XP Beckman Coulter ultracentrifuge. The supernatants were removed. The crude ribosome pellets were washed with 500 μl wash buffer (25 mM potassium Hepes pH 7.2, 400 mM potassium acetate, 15 mM magnesium acetate, 200 μM CHX, 1 mM DTT, 0.1 mM AEBSF, 10 U/ml RNase inhibitor) three times. After washing, the crude ribosome pellets were then resuspended in 200 μl of lysis buffer. The resuspensions were again layered over 1 ml of 1 M sucrose cushion and the pelleting repeated as above. Washing was repeated as previous. The crude ribosome pellets used in polysome profiling were then resuspended in 200 μl of ribosome resuspension buffer and, if not immediately used, flash frozen in liquid nitrogen and stored at –80 °C for later use. Crude ribosome pellets used for immunoblotting were resuspended in sample buffer at 37 °C for 20 min, boiled at 95 °C for 5 min, and chilled on ice. Sucrose gradients were generated using polysome profiling buffer (25 mM potassium Hepes pH 7.2, 400 mM potassium acetate, 15 mM magnesium acetate, 200 μM CHX, 1 mM DTT, 1 mM AEBSF) with 10%, 20%, 30%, 40%, and 50% (w/v) sucrose layers in 14 mm x 89 mm polyallomer centrifuge tubes (Beckman #331372). Total RNA of resuspended crude ribosomes was measured to ensure a minimum of 300 μg total was loaded onto the gradient. Samples were layered over the gradient and balanced using polysome profiling buffer. The gradients were centrifuged at 35,000 RPM (acceleration 3, deceleration 4) for 2 h and 40 min at 4 °C using an Optima L-100 XP Beckman Coulter ultracentrifuge in a SW41 swing bucket rotor. Centrifuged gradients were then fractionated using a density gradient fractionation system (BRANDEL #BR188176). Samples were collected into 1.7 ml microcentrifuge tubes with an equal volume of Ribozol (VWR #VWRVN580) with 1% (w/v) SDS for RNA or three volumes of 20% (v/v) TCA in MilliQ water for protein. Samples were mixed by vortexing. RNA was stored at –80 °C if not isolated immediately. RNA was isolated following manufacturer protocol and used in RNA gel electrophoresis. Protein samples were stored or incubated at 4 °C overnight to precipitate protein. Samples were then centrifuged at 20,000*g*, 4 °C for 30 min. Supernatant was removed.

The pellets were washed with 100% acetone twice. Pellets were then solubilized in sample buffer for Western blot analysis.

Crude ribosome pellets and polysome profiling in mammalian cells was done based on previous work (62). HAP1 cells were grown to 80 to 90% confluency in a 10 cm dish. Cells were washed three times with 5 ml of ice-cold PBS + 200 μM CHX. A 400 μl volume of lysis buffer (20 mM Tris–HCl pH 7.4, 150 mM NaCl, 5 mM MgCl₂, 1% (v/v) Triton X-100, 200 μM CHX, 1 mM DTT, 1 mM AEBSF, 40 U/ml RNase inhibitor) was then added dropwise to the place and the cells were scraped off and collected into a 1.7 ml microcentrifuge tube. The lysate was pipetted several times and incubated on ice for 10 min. The samples were then centrifuged at 20,000*g* for 10 min at 4 °C to remove cell debris. The lysate was transferred into a new tube. If not used immediately, lysates were flash frozen in liquid nitrogen and stored at –80 °C. Crude ribosome pellets were generated by layering 200 μl of lysate over 0.9 ml of 1M sucrose cushion (1 M sucrose, 20 mM Tris–HCl pH 7.4, 150 mM NaCl, 5 mM MgCl₂, 200 μM CHX, 1 mM DTT, 1 mM AEBSF, 40 U/ml RNase inhibitor). The balanced tubes were then placed in a TLA 100.3 rotor and centrifuged for 1 h at 100,000*g* at 4 °C using an Optima Max-XP Beckman Coulter ultracentrifuge. The supernatants were removed. The crude ribosome pellets were washed with 500 μl wash buffer (20 mM Tris–HCl pH 7.4, 150 mM NaCl, 5 mM MgCl₂, 0.1% (v/v) Tween 20, 200 μM CHX, 1 mM DTT, 0.1 mM AEBSF, 10 U/ml RNase inhibitor) three times. Crude ribosome pellets used for immunoblotting were resuspended in sample buffer at 37 °C for 20 min, boiled at 95 °C for 5 min, and chilled on ice. Polysome profiling was performed by layering clarified HAP1 cell lysates over sucrose gradient generated with polysome profiling buffer (20 mM Tris–HCl pH 7.4, 150 mM NaCl, 5 mM MgCl₂, 200 μM CHX, 1 mM DTT, 1 mM AEBSF, 40 U/ml RNase inhibitor) and centrifugation was performed as above. Samples were collected and isolated at above for RNA gel electrophoresis and Western blot analysis.

HA-immunoprecipitation and immunoblotting

Mixed *P. falciparum* Dd2 parasites were harvested at 7 to 10% parasitemia. For examination of RACK1 variant expression, parasites were released from red blood cells by saponin lysis as previously described. Parasites were then lysed using passive lysis buffer (Promega #E1910) and the total protein concentration was calculated by RC/DC kit (BioRad #5000122). For each reaction, 25 μl of magnetic anti-HA beads (Thermo Scientific™) was washed twice in 1X PBS with 0.1% (v/v) Tween 20 and then twice in binding buffer (50 mM Tris pH7.5, 150 mM NaCl, 1% (v/v) IGEPAL CA-630, 5% (v/v) glycerol, and protease inhibitors (Thermo Fisher #A32955): apoptin, leupeptin, bestatin, E-64, AEBSF, pepstatin A). A total of 500 μg of protein was loaded onto the HA beads and bound overnight at 4 °C. The beads were then washed three times with 1 ml of wash buffer (50 mM Tris pH7.5, 150 mM NaCl, 1% (v/v) IGEPAL CA-630, 5% (v/v) glycerol). Beads were then eluted in 50 μl of sample buffer and examined by Western blot analysis.

Samples were loaded onto SDS-PAGE gels, running at 15 W, 1 h 10 min. The gels were then transferred to PVDF membrane using semi-dry transfer method running at 25 V for 40 min. The PVDF membranes were blocked in 5% (w/v) milk in PBS + 0.1% (v/v) Tween 20 (PBST) for 1 h at room temperature or overnight at 4 °C. The membranes were probed with diluted primary antibody in PBST with 5% (w/v) milk. After incubation with the primary antibody, the PVDF membranes were washed three times for 5 min in PBST. Membranes incubated with horseradish peroxidase–conjugated primaries were incubated and washed similarly, washing with PBST, and then proceeding to imaging instead of secondary. The membranes were then incubated with horseradish peroxidase–conjugated secondary antibody diluted 1:2500 in PBST with 5% (w/v) milk for 1 h at room temperature. The membranes were washed as above and then rinsed with PBS. Working Solution was prepared by mixing equal parts of the Stable Peroxide Solution and the Luminol/Enhancer Solution (34577 SuperSignal West Pico PLUS, 34096 SuperSignal West Femto Maximum Sensitivity Substrate, respectively). We incubate the blot in Working Solution for 5 min. The blot from Working Solution was removed and the excess reagent was drained. Afterward, we took images that were generated by BioRad Molecular Imager ChemiDoc XRS System with Image Lab software.

qPCR analysis of polysome rRNA and rRNA bound to RACK1 variant

RNA isolated from polysome profiling fractions was analyzed by qPCR. Using the NanoDrop 2000c, 50 ng of total RNA was used to generate cDNA *via* the iScript Advance cDNA Kit for RT-qPCR (BioRAD #1725037), for each sample including no reverse transcriptase and no template controls following the manufacturer's protocol. The iTaq Universal SYBR Green Supermix (BioRAD #1725121) protocol was used for qRT-PCR on the CFX96 Real-Time system with Bio-Rad CFX Manager 3.0 software (63). The 2^{-Ct} value were calculated and plotted for each fraction.

HA-immunoprecipitation was performed on parasite crude ribosome pellets, both previously described. The total protein concentration in each crude ribosome pellet was calculated by RC/DC kit (BioRad #5000122). The beads were then blocked with polysome parasite lysis buffer containing 4% (w/v) bovine serum albumin and 0.5 µg/ml *S. cerevisiae* tRNAs for 1 h at 4 °C while rotating. A total of 680 µg of protein was loaded onto the HA beads and bound for 1 h at 4 °C while rotating. The beads were then washed three times with 1 ml of polysome wash buffer. Beads were split in half. For protein, beads were then eluted in 35 µl of sample buffer and examined by Western blot analysis as previously described. For RNA, beads were eluted with 400 µl Trizol + 1% (w/v) SDS at 36 °C while shaking. RNA was isolated per the manufacturer's protocol. Using the NanoDrop 2000c, 50 ng of total RNA was used to generate cDNA *via* the iScript Advance cDNA Kit for RT-qPCR (BioRAD #1725037), for each sample including no reverse transcriptase and no template controls following the

manufacturer's protocol. The iTaq Universal SYBR Green Supermix (BioRAD #1725121) protocol was used for qRT-PCR on the CFX96 Real-Time system with Bio-Rad CFX Manager 3.0 software (63). The ΔCt was calculated by subtracting the Dd2 parent line values from each sample. The ΔΔCt value was then calculated by normalization to the WT PfRACK1 variant. Plots were then generated using the calculated $2^{-\Delta\Delta Ct}$ values for each variant.

Data availability

All the data and procedures are contained within the article. Original files for images, qPCR, and models can be shared upon request to Dr Sergej Djuranovic (sergej.djuranovic@wustl.edu).

References

1. Adams, D. R., Ron, D., and Kiely, P. A. (2011) RACK1, A multifaceted scaffolding protein: Structure and function. *Cell Commun. Signal.* **9**, 22
2. Jain, B. P., and Pandey, S. (2018) WD40 repeat proteins: Signalling scaffold with diverse functions. *Protein J.* **37**, 391–406
3. Li, D., and Roberts, R. (2001) Human genome and diseases: WD-repeat proteins: Structure characteristics, biological function, and their involvement in human diseases. *Cell Mol. Life Sci.* **58**, 2085–2097
4. Ron, D., Chen, C. H., Caldwell, J., Jamieson, L., Orr, E., and Mochly-Rosen, D. (1994) Cloning of an intracellular receptor for protein

kinase C: A homolog of the beta subunit of G proteins. *Proc. Natl. Acad. Sci. U. S. A.* **91**, 839–843

5. Yuan, L., Su, Y., Zhou, S., Feng, Y., Guo, W., and Wang, X. (2017) A RACK1-like protein regulates hyphal morphogenesis, root entry and *in vivo* virulence in Verticillium dahliae. *Fungal Genet. Biol.* **99**, 52–61

6. Bradford, W., Buckholz, A., Morton, J., Price, C., Jones, A. M., and Urano, D. (2013) Eukaryotic G protein signaling evolved to require G protein-coupled receptors for activation. *Sci. Signal.* **6**, ra37

7. Smith, B. L., and Mochly-Rosen, D. (1992) Inhibition of protein kinase C function by injection of intracellular receptors for the enzyme. *Biochem. Biophys. Res. Commun.* **188**, 1235–1240

8. Johnson, A. G., Lapointe, C. P., Wang, J., Corsepius, N. C., Choi, J., Fuchs, G., and Puglisi, J. D. (2019) RACK1 on and off the ribosome. *RNA* **25**, 881–895

9. Gallo, S., Ricciardi, S., Manfrini, N., Pesce, E., Oliveto, S., Calamita, P., Mancino, M., Maffioli, E., Moro, M., Crosti, M., Berno, V., Bombaci, M., Tedeschi, G., and Biffo, S. (2018) RACK1 specifically regulates translation through its binding to ribosomes. *Mol. Cell Biol.* **38**, e00230-18

10. Sengupta, J., Nilsson, J., Gursky, R., Spahn, C. M., Nissen, P., and Frank, J. (2004) Identification of the versatile scaffold protein RACK1 on the eukaryotic ribosome by cryo-EM. *Nat. Struct. Mol. Biol.* **11**, 957–962

11. Thompson, M. K., Rojas-Duran, M. F., Gangaramani, P., and Gilbert, W. V. (2016) The ribosomal protein Asc1/RACK1 is required for efficient translation of short mRNAs. *Elife* **5**, e11154

12. Nilsson, J., Sengupta, J., Frank, J., and Nissen, P. (2004) Regulation of eukaryotic translation by the RACK1 protein: A platform for signalling molecules on the ribosome. *EMBO Rep.* **5**, 1137–1141

13. Kouba, T., Rutkai, E., Karásková, M., and Valášek, L. (2012) The eIF3c/NIP1 PCI domain interacts with RNA and RACK1/ASC1 and promotes assembly of translation preinitiation complexes. *Nucl. Acids Res.* **40**, 2683–2699

14. Ceci, M., Gaviraghi, C., Gorrini, C., Sala, L. A., Offenhäuser, N., Marchisio, P. C., and Biffo, S. (2003) Release of eIF6 (p27BBP) from the 60S subunit allows 80S ribosome assembly. *Nature* **426**, 579–584

15. Sugiyama, T., Li, S., Kato, M., Ikeuchi, K., Ichimura, A., Matsuo, Y., and Inada, T. (2019) Sequential ubiquitination of ribosomal protein uS3 triggers the degradation of non-functional 18S rRNA. *Cell Rep.* **26**, 3400–3415.e7

16. Joazeiro, C. A. P. (2017) Ribosomal stalling during translation: Providing substrates for ribosome-associated protein quality control. *Annu. Rev. Cell Dev. Biol.* **33**, 343–368

17. Kuroha, K., Akamatsu, M., Dimitrova, L., Ito, T., Kato, Y., Shirahige, K., and Inada, T. (2010) Receptor for activated C kinase 1 stimulates nascent polypeptide-dependent translation arrest. *EMBO Rep.* **11**, 956–961

18. Ikeuchi, K., Yazaki, E., Kudo, K., and Inada, T. (2016) Conserved functions of human Pelota in mRNA quality control of nonstop mRNA. *FEBS Lett.* **590**, 3254–3263

19. Sundaramoorthy, E., Leonard, M., Mak, R., Liao, J., Fulzele, A., and Bennett, E. J. (2017) ZNF598 and RACK1 regulate mammalian ribosome-associated quality control function by mediating regulatory 40S ribosomal ubiquitylation. *Mol. Cell* **65**, 751–760.e4

20. Blomqvist, K., DiPetrillo, C., Streva, V. A., Pine, S., and Dvorin, J. D. (2017) Receptor for Activated C-Kinase 1 (PfRACK1) is required for Plasmodium falciparum intra-erythrocytic proliferation. *Mol. Biochem. Parasitol.* **211**, 62–66

21. Vincensini, L., Richert, S., Blisnick, T., Van Dorsselaer, A., Leize-Wagner, E., Rabilloud, T., and Braun Breton, C. (2005) Proteomic analysis identifies novel proteins of the maurer's clefts, a secretory compartment delivering Plasmodium falciparum proteins to the surface of its host cell. *Mol. Cell Proteomics* **4**, 582–593

22. Wong, W., Bai, X. C., Brown, A., Fernandez, I. S., Hanssen, E., Condron, M., Tan, Y. H., Baum, J., and Scheres, S. H. (2014) Cryo-EM structure of the Plasmodium falciparum 80S ribosome bound to the anti-protozoan drug emetine. *Elife* **3**, e03080

23. Sun, M., Li, W., Blomqvist, K., Das, S., Hashem, Y., Dvorin, J. D., and Frank, J. (2015) Dynamical features of the Plasmodium falciparum ribosome during translation. *Nucl. Acids Res.* **43**, 10515–10524

24. Bunnik, E. M., Batugedara, G., Saraf, A., Prudhomme, J., Florens, L., and Le Roch, K. G. (2016) The mRNA-bound proteome of the human malaria parasite Plasmodium falciparum. *Genome Biol.* **17**, 147

25. Coyle, S. M., Gilbert, W. V., and Doudna, J. A. (2009) Direct link between RACK1 function and localization at the ribosome *in vivo*. *Mol. Cell Biol.* **29**, 1626–1634

26. Rollins, M. G., Jha, S., Bartom, E. T., and Walsh, D. (2019) RACK1 evolved species-specific multifunctionality in translational control through sequence plasticity within a loop domain. *J. Cell Sci.* **132**, jcs228908

27. Waterhouse, A., Bertoni, M., Bienert, S., Studer, G., Tauriello, G., Gumienny, R., Heer, F. T., de Beer, T. A. P., Rempfer, C., Bordoli, L., Lepore, R., and Schwede, T. (2018) SWISS-MODEL: Homology modelling of protein structures and complexes. *Nucl. Acids Res.* **46**, W296–W303

28. Bienert, S., Waterhouse, A., de Beer, T. A., Tauriello, G., Studer, G., Bordoli, L., and Schwede, T. (2017) The SWISS-MODEL Repository—new features and functionality. *Nucl. Acids Res.* **45**, D313–D319

29. Guex, N., Peitsch, M. C., and Schwede, T. (2009) Automated comparative protein structure modeling with SWISS-model and Swiss-PdbViewer: A historical perspective. *Electrophoresis* **30**, S162–S173

30. Studer, G., Rempfer, C., Waterhouse, A. M., Gumienny, R., Haas, J., and Schwede, T. (2020) QMEANDisCo—distance constraints applied on model quality estimation. *Bioinformatics* **36**, 1765–1771

31. Bertoni, M., Kiefer, F., Biasini, M., Bordoli, L., and Schwede, T. (2017) Modeling protein quaternary structure of homo- and hetero-oligomers beyond binary interactions by homology. *Sci. Rep.* **7**, 10480

32. Jumper, J., Evans, R., Pritzel, A., Green, T., Figurnov, M., Ronneberger, O., Tunyasuvunakool, K., Bates, R., Žídek, A., Potapenko, A., Bridgland, A., Meyer, C., Kohl, S. A. A., Ballard, A. J., Cowie, A., *et al.* (2021) Highly accurate protein structure prediction with AlphaFold. *Nature* **596**, 583–589

33. Varadi, M., Anyango, S., Deshpande, M., Nair, S., Natassia, C., Yordanova, G., Yuan, D., Stroe, O., Wood, G., Laydon, A., Žídek, A., Green, T., Tunyasuvunakool, K., Petersen, S., Jumper, J., *et al.* (2022) AlphaFold protein structure database: Massively expanding the structural coverage of protein-sequence space with high-accuracy models. *Nucl. Acids Res.* **50**, D439–D444

34. Nielsen, M. H., Flygaard, R. K., and Jenner, L. B. (2017) Structural analysis of ribosomal RACK1 and its role in translational control. *Cell. Signal.* **35**, 272–281

35. López-Barragán, M. J., Lemieux, J., Quiñones, M., Williamson, K. C., Molina-Cruz, A., Cui, K., Barillas-Mury, C., Zhao, K., and Su, X. Z. (2011) Directional gene expression and antisense transcripts in sexual and asexual stages of Plasmodium falciparum. *BMC Genomics* **12**, 587

36. Aurrecoechea, C., Brestelli, J., Brunk, B. P., Dommer, J., Fischer, S., Gajria, B., Gao, X., Gingle, A., Grant, G., Harb, O. S., Heiges, M., Innamorato, F., Iodice, J., Kissinger, J. C., Kraemer, E., *et al.* (2009) PlasmoDB: A functional genomic database for malaria parasites. *Nucl. Acids Res.* **37**, D539–D543

37. Pease, B. N., Huttlin, E. L., Jedrychowski, M. P., Talevich, E., Harmon, J., Dillman, T., Kannan, N., Doerig, C., Chakrabarti, R., Gygi, S. P., and Chakrabarti, D. (2013) Global analysis of protein expression and phosphorylation of three stages of Plasmodium falciparum intraerythrocytic development. *J. Proteome Res.* **12**, 4028–4045

38. Jha, S., Rollins, M. G., Fuchs, G., Procter, D. J., Hall, E. A., Cozzolino, K., Sarnow, P., Savas, J. N., and Walsh, D. (2017) Trans-kingdom mimicry underlies ribosome customization by a poxvirus kinase. *Nature* **546**, 651–655

39. Warner, J. R. (1977) In the absence of ribosomal RNA synthesis, the ribosomal proteins of HeLa Cells are synthesized normally and degraded rapidly. *J. Mol. Biol.* **115**, 315–333

40. von Bohl, A., Kuehn, A., Simon, N., Ngongang, V. N., Spehr, M., Baumeister, S., Przyborski, J. M., Fischer, R., and Pradel, G. (2015) A WD40-repeat protein unique to malaria parasites associates with adhesion protein complexes and is crucial for blood stage progeny. *Malar. J.* **14**, 435

41. Salmon, B. L., Oksman, A., and Goldberg, D. E. (2001) From the cover: Malaria parasite exit from the host erythrocyte: A two-step process requiring extraerythrocytic proteolysis. *Proc. Natl. Acad. Sci. U. S. A.* **98**, 271–276

42. Glushakova, S., Mazar, J., Hohmann-Marriott, M. F., Hama, E., and Zimmerberg, J. (2009) Irreversible effect of cysteine protease inhibitors on the release of malaria parasites from infected erythrocytes. *Cell Microbiol.* **11**, 95–105

43. Hale, V. L., Watermeyer, J. M., Hackett, F., Vizcay-Barrena, G., van Ooij, C., Thomas, J. A., Spink, M. C., Harkiolaki, M., Duke, E., Fleck, R. A., Blackman, M. J., and Saibil, H. R. (2017) Parasitophorous vacuole poration precedes its rupture and rapid host erythrocyte cytoskeleton collapse in Plasmodium falciparum egress. *Proc. Natl. Acad. Sci. U. S. A.* **114**, 3439–3444

44. Regmi, S., Rothberg, K. G., Hubbard, J. G., and Ruben, L. (2008) The RACK1 signal anchor protein from trypanosoma brucei associates with eukaryotic elongation factor 1A: A role for translational control in cytokinesis. *Mol. Microbiol.* **70**, 724–745

45. Lacsina, J. R., LaMonte, G., Nicchitta, C. V., and Chi, J. T. (2011) Polysome profiling of the malaria parasite Plasmodium falciparum. *Mol. Biochem. Parasitol.* **179**, 42–46

46. Caro, F., Ahyong, V., Betegon, M., and DeRisi, J. L. (2014) Genome-wide regulatory dynamics of translation in the Plasmodium falciparum asexual blood stages. *Elife* **3**, e04106

47. Zanghì, G., Vembar, S. S., Baumgarten, S., Ding, S., Guizetti, J., Bryant, J. M., Mattei, D., Jensen, A. T. R., Rénia, L., Goh, Y. S., Sauerwein, R., Hermsen, C. C., Franetich, J. F., Bordessoulles, M., Silvie, O., *et al.* (2018) A specific PfEMP1 is expressed in P. Falciparum sporozoites and plays a role in hepatocyte infection. *Cell Rep.* **22**, 2951–2963

48. Ruiz Carrillo, D., Chandrasekaran, R., Nilsson, M., Cornvik, T., Liew, C. W., Tan, S. M., and Lescar, J. (2012) Structure of human Rack1 protein at a resolution of 2.45 Å. *Acta Crystallogr. Sect. F Struct. Biol. Cryst. Commun.* **68**, 867–872

49. Altschul, S. F., Wootton, J. C., Gertz, E. M., Agarwala, R., Morgulis, A., Schäffer, A. A., and Yu, Y. K. (2005) Protein database searches using compositionally adjusted substitution matrices. *FEBS J.* **272**, 5101–5109

50. Altschul, S. F., Madden, T. L., Schäffer, A. A., Zhang, J., Zhang, Z., Miller, W., and Lipman, D. J. (1997) Gapped BLAST and PSI-BLAST: A new generation of protein database search programs. *Nucl. Acids Res.* **25**, 3389–3402

51. Zimmermann, L., Stephens, A., Nam, S. Z., Rau, D., Kübler, J., Lozajic, M., Gabler, F., Söding, J., Lupas, A. N., and Alva, V. (2018) A completely reimplemented MPI bioinformatics toolkit with a new HHpred server at its core. *J. Mol. Biol.* **430**, 2237–2243

52. Klausen, M. S., Jespersen, M. C., Nielsen, H., Jensen, K. K., Jurtz, V. I., Sønderby, C. K., Sommer, M. O. A., Winther, O., Nielsen, M., Petersen, B., and Marcatili, P. (2019) NetSurfP-2.0: Improved prediction of protein structural features by integrated deep learning. *Proteins* **87**, 520–527

53. Hanson, J., Yang, Y., Paliwal, K., and Zhou, Y. (2016) Improving protein disorder prediction by deep bidirectional long short-term memory recurrent neural networks. *Bioinformatics* **33**, 685–692

54. Jones, D. T., and Cozzetto, D. (2015) DISOPRED3: Precise disordered region predictions with annotated protein-binding activity. *Bioinformatics* **31**, 857–863

55. Yan, R., Xu, D., Yang, J., Walker, S., and Zhang, Y. (2013) A comparative assessment and analysis of 20 representative sequence alignment methods for protein structure prediction. *Sci. Rep.* **3**, 2619

56. Heffernan, R., Yang, Y., Paliwal, K., and Zhou, Y. (2017) Capturing non-local interactions by long short-term memory bidirectional recurrent neural networks for improving prediction of protein secondary structure, backbone angles, contact numbers and solvent accessibility. *Bioinformatics* **33**, 2842–2849

57. Jones, D. T. (1999) Protein secondary structure prediction based on position-specific scoring matrices 1 1Edited by G. Von Heijne. *J. Mol. Biol.* **292**, 195–202

58. Brown, A., Shao, S., Murray, J., Hegde, R. S., and Ramakrishnan, V. (2015) Structural basis for stop codon recognition in eukaryotes. *Nature* **524**, 493–496

59. Jurrus, E., Engel, D., Star, K., Monson, K., Brandi, J., Felberg, L. E., Brookes, D. H., Wilson, L., Chen, J., Liles, K., Chun, M., Li, P., Gohara, D. W., Dolinsky, T., Konecny, R., *et al.* (2018) Improvements to the APBS biomolecular solvation software suite. *Protein Sci.* **27**, 112–128

60. Trager, W., and Jensen, J. B. (2005) Human malaria parasites in continuous culture. 1976. *J. Parasitol.* **91**, 484–486

61. Fidock, D. A., and Wellems, T. E. (1997) Transformation with human dihydrofolate reductase renders malaria parasites insensitive to WR99210 but does not affect the intrinsic activity of proguanil. *Proc. Natl. Acad. Sci. U. S. A.* **94**, 10931–10936

62. McGlincy, N. J., and Ingolia, N. T. (2017) Transcriptome-wide measurement of translation by ribosome profiling. *Methods* **126**, 112–129

63. Arthur, L., Pavlovic-Djuranovic, S., Smith-Koutmou, K., Green, R., Szczesny, P., and Djuranovic, S. (2015) Translational control by lysine-encoding A-rich sequences. *Sci. Adv.* **1**, e1500154

≋ASBMB